

¹ Explicit and Mean-Field Models for Coverage-Dependent CO
² Adsorption on Pd(111)

³ John P. Clay,^a Steven J. McDonough,^a Kurt Frey,^a Jeffrey P. Greeley,^b Fabio H. Ribeiro,^b
W. Nicholas Delgass,^b and William F. Schneider^{a,c*}

⁴ ^a Department of Chemical and Biomolecular Engineering. 182 Fitzpatrick Hall. University of
⁵ Notre Dame. Notre Dame, IN 46556. USA

⁶ ^b School of Chemical Engineering. 480 Stadium Mall Drive. Purdue University. West Lafayette,
⁷ IN 47907. USA

⁸ ^c Department of Chemistry and Biochemistry. 251 Nieuwland Science Hall. University of Notre
⁹ Dame. Notre Dame, IN 46556. USA

¹⁰

*Corresponding author: wschneider@nd.edu, +1-574-631-8754

11 **Introduction**

12 **Highlight**

- 13 1. Developed one,two,three site cluster expansion model for Pd(111)-CO system.
- 14 2. Extract coverage-dependent CO binding energy on Pd from finite temperature Monte
- 15 Carlo simulation (GCMC).

$$\bar{E}_{\text{CO}}(\theta, T) = \mu_{\text{CO}}(\theta, T) + T\bar{S}_{\text{CO}}(\theta, T) \quad (1)$$

$$\bar{S}_{\text{CO}}(\theta, T) = -k_B T \ln \left(\frac{\theta}{n * (1 - \theta)} \right) \quad (2)$$

- 16 3. Obtain analytical expression of coverage dependent binding energy $\bar{E}(\theta)$.
- 17 4. Simulated CO TPD with analytical expression of $\bar{E}(\theta)$ consistent with experimental TPD.

$$r_{\text{Des}} = -\frac{\partial \theta}{\partial T} = \nu * \theta * \exp \left(\frac{\bar{E}_{\text{CO}}(\theta)}{k_B T} \right) \quad (3)$$

18 **Justification**

- 19 1. CO adsorption step is crucial in WGS reaction process. Adsorption site and adsorbates
20 interaction can effect binding energy of CO. From volcano plot, binding enrgy related
21 to catalyst activity. Capturing binding energy will contribute to better prediction of
22 temperature programmed desorption (TPD) spectra and even to reliable microkinetic
23 model.
- 24 2. Conventionally, DFT method was used to compute binding energy with certain coverage
25 and configuration, or fitting function for formation energy vs. coverage and then take
26 derivative. But it would be impractical to compute binding energy of all coverages and
27 configurations.
- 28 3. An alternative method to represent DFT energy is Cluster Expansion(CE). CE is a poly-
29 nomial form that can express energy by given configuration. CE model can be trained
30 by DFT database and once it reach convergence, CE will be used as Hamiltonian to
31 perform Monte Carlo simulation. GCMC simulation take advantage of fixed chemical

32 potential (μ), temperature (T) and number of particles(N), large supercell and metropolis
33 algorithm until system reach to specified convergence.

34 4. Having analytical expression of $\bar{E}_{CO}(\theta)$ will be convenient to predict TPD spectra from
35 equation 3 with Euler forward integration.

36 **Guide To Reader**

37 Here we combine cluster expansion and Grand Canonical Monte Carlo (GCMC) simulation to
38 extract coverage-dependent binding energy of CO on Pd (111). We explore how different CE
39 model impact binding energy with various temperature. Three model are used to fit simulation
40 result to obtain analytical expression of binding energy with respect to coverage, piecewise[1],
41 activity [2] and logistic[3]. Then simulated TPD can be generated by those model. We compare
42 simulated TPD with experimental TPD [4] to confirm our approach can accurately model TPD
43 spectra.

Piece-wise linear: $\bar{E}_{CO}(\theta) = A$ for $\theta < C$ and $A + B(\theta - C)$ for $\theta \geq C$

$$\text{Activity: } \bar{E}_{CO}(\theta) = A + B \left\{ \frac{\lambda_1}{1 + \lambda_1 \theta} + \ln \left(\frac{1 + \lambda_2 \theta}{1 + \lambda_1 \theta} \right) + \theta \left[\frac{\lambda_2 - \lambda_1}{(1 + \lambda_2 \theta)(1 + \lambda_1 \theta)} \right] \right\}$$

$$\text{Logistic: } \bar{E}_{CO}(\theta) = \frac{A}{B \exp(C\theta) + D}$$

⁴⁴ Results and Discussion

⁴⁵ Pd(111) Surface

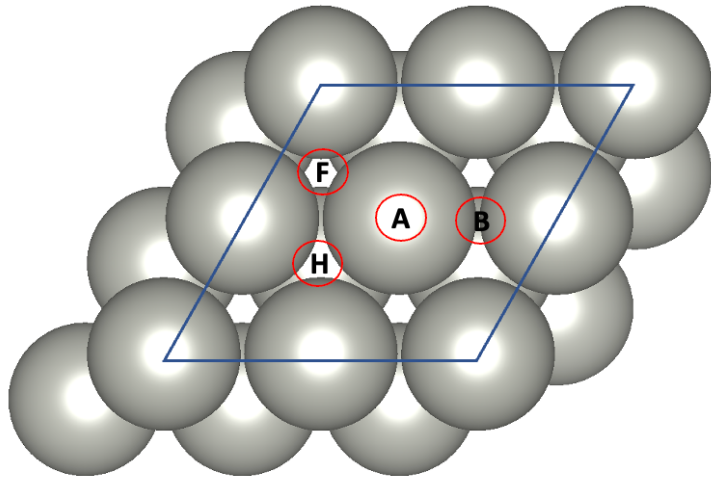


Figure 1: Geometric relationship between FCC, HCP, and ATOP sites in the (2×2) supercell (black lines) on the (111) surface of a close-packed metal. (F), (H), and (A) represent FCC, HCP, ATOP sites, respectively.

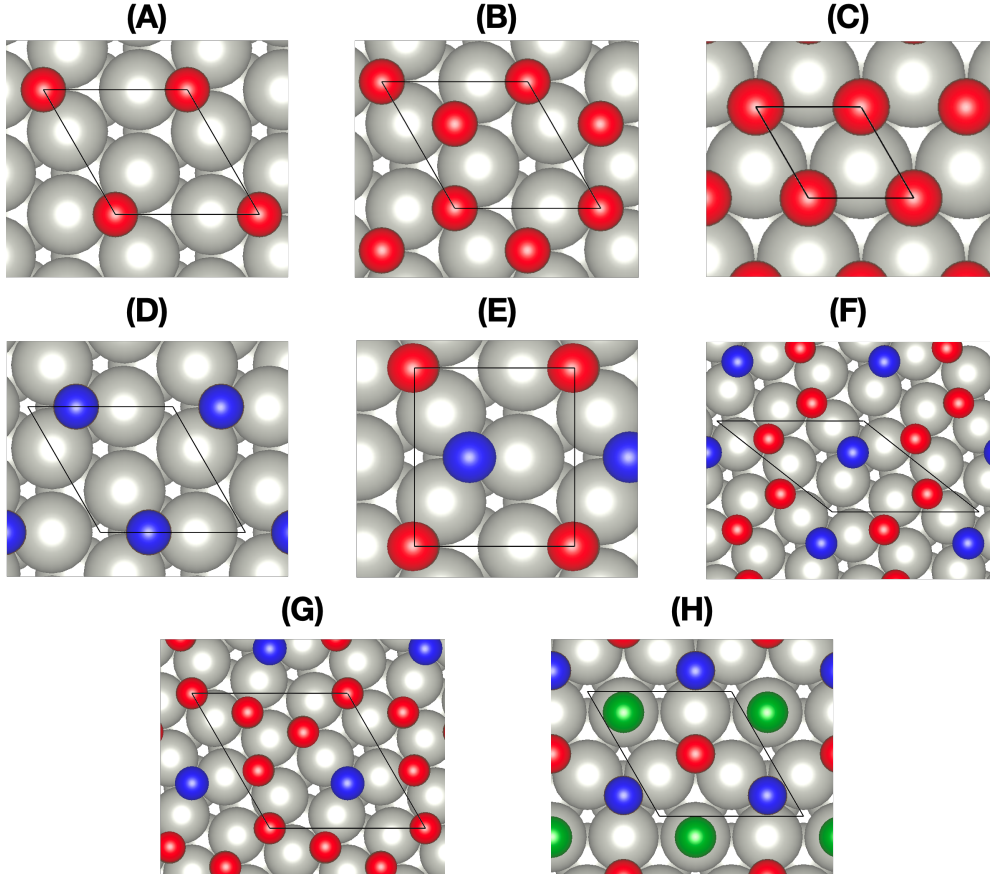


Figure 2: Top view of computed ground state structures. Red, blue and green correspond to FCC, HCP, and ATOP sites, respectively. (A) 1/3 ML FCC, (B) 2/3 ML FCC, (C) 1 ML FCC, (D) 1/3 ML HCP Hollow, (E) 1/2 ML FCC/HCP, (F) 3/5 ML FCC/HCP, (G) 5/7 ML FCC/HCP, and (H) 3/4 ML FCC/HCP/ATOP. Black lines represent the unit cell.

Table 1: Geometric Data for the FCC Hollow Site Cluster Expansion Ground States.

Coverage (ML)	Geometry
1/3	$(\sqrt{3} \times \sqrt{3})R30^\circ - 1$ CO
2/3	$(\sqrt{3} \times \sqrt{3})R30^\circ - 2$ CO
1	(1×1) -1 CO

Table 2: Geometric Data for the FCC and HCP Hollow Site Cluster Expansion Ground States.

Coverage (ML)	Geometry
1/3	$(\sqrt{3} \times \sqrt{3})R30^\circ - 1$ CO
1/2	c(4×2)–2 CO
3/5	$ a = b = 7.399 \text{ \AA}$, $\psi=141.78^\circ$
5/7	$ a = b = 7.399 \text{ \AA}$, $\psi=120.00^\circ$
1	(1×1)–1 CO

Table 3: Geometric Data for the FCC, HCP Hollow, and Atop Site Cluster Expansion Ground States.

Coverage (ML)	Geometry
1/3	$(\sqrt{3} \times \sqrt{3})R30^\circ - 1$ CO
1/2	c(4×2)–2 CO
3/5	$ a = b = 7.399 \text{ \AA}$, $\psi=141.78^\circ$
3/4	(2×2) – 3 CO
1	(1×1)–1 CO

47 Cluster Expansion

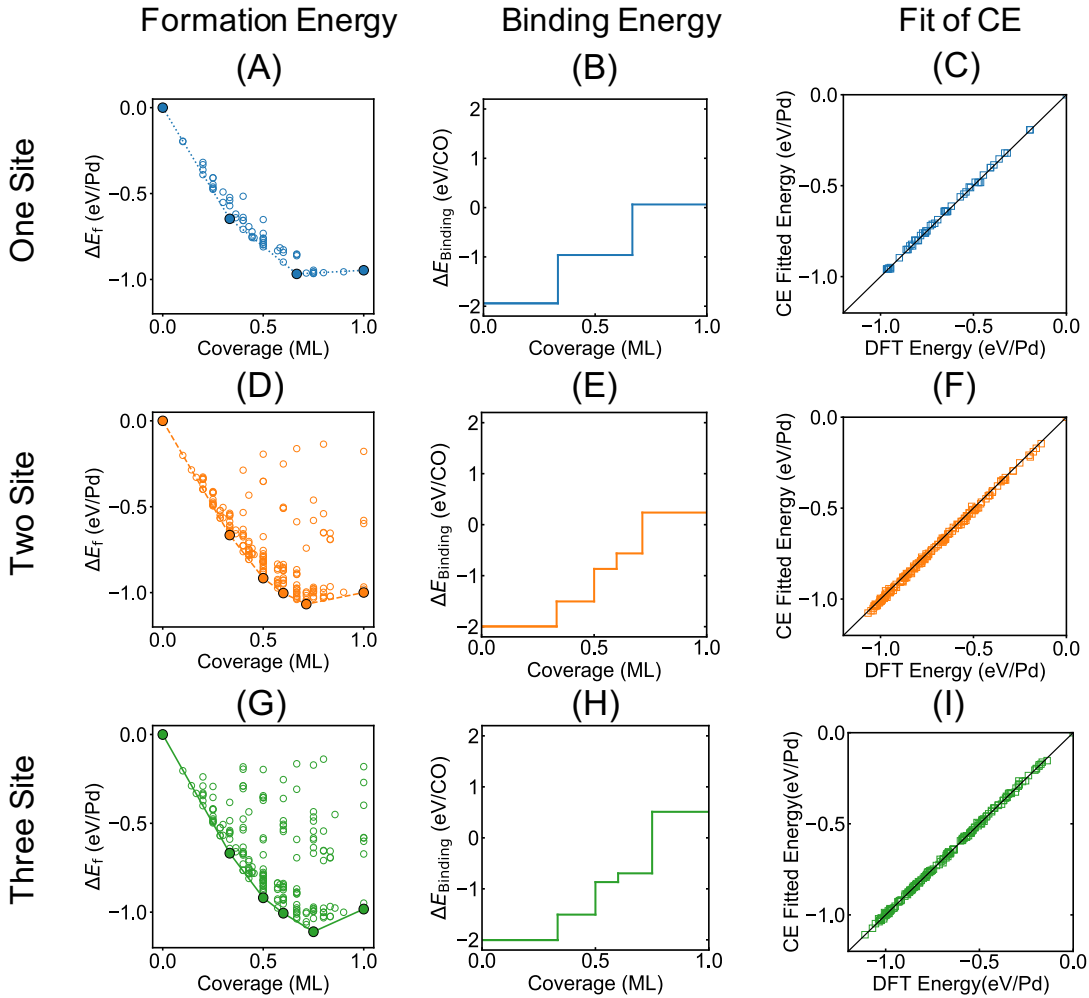


Figure 3: First column: GGA-computed formation energies vs. coverage for FCC-only, FCC/HCP, and FCC/HCP/atop models from top to bottom. Middle column: differential binding energy vs. coverage for same three models. Last column: CE fitted vs. DFT-computed formation energies for same three models.

- 48 1. Figure 3 C compares the GGA-computed formation energies with the CE predictions.
 49 The two-body-only CE fits the data with a cross validation score of 7.59 meV/Å². Figure
 50 3 A shows the DFT-computed formation energies. The minimum energy hull has two
 51 “kinks” at 1/3 and 2/3 ML corresponding to a $(\sqrt{3} \times \sqrt{3})R30^\circ - 1$ CO (Figure 2 A) and
 52 a $(\sqrt{3} \times \sqrt{3})R30^\circ - 2$ CO configuration (Figure 2 B), respectively. Figure 2 C includes
 53 for completeness the (1 × 1) structure. The slope of the formation energy hull is the 0 K
 54 differential binding energy, $\bar{E}_{\text{CO}}^{\text{FCC}}(\theta, 0 \text{ K})$, and is plotted in Figure 3 B. The 0 K differential
 55 binding energy is constant to 1/3 ML, up to which coverage each adsorbate can avoid any
 56 first nearest neighbor (1NN) interactions, steps up above 1/3 ML as each new adsorbate

57 accumulates three 1NNs, and steps up again to a positive value above 2/3 ML, where each
58 new adsorbate acquires 6 1NNs.

- 59 2. The inclusion of FCC and HCP sites together yields a richer formation energy hull, shown
60 in Figure 3 D. The ground state at 1/3 ML remains and has the same $(\sqrt{3} \times \sqrt{3})R30^\circ - 1$
61 CO structure, although as expected from the comparisons in Table 1, with CO in HCP
62 sites (Figure 2 D). A new ground state appears at 1/2 ML in which half the CO occupy
63 FCC and half HCP sites, each CO sublattice having c(4 × 2) symmetry (Figure 2 E). In
64 this configuration half the surface Pd have two CO in opposing (second nearest neighbor,
65 2NN) FCC and HCP sites and the other half have either a single FCC or HCP CO.
66 Another new ground state appears at 3/5 ML (Figure 2 F) in which 2/3 of the CO occupy
67 FCC and 1/3 HCP sites. Here the FCC CO form chains of adjacent occupied sites like
68 that in the 2/3 ML FCC-only structure, with the chains separated by intervening rows of
69 HCP CO. The more dense 2/3 ML FCC-only ground state disappears in the FCC/HCP
70 system. In its place appears a 5/7 ML structure (Figure 2 G) in which 4/5 of the CO
71 occupy FCC and 1/5 HCP sites. The structure is more complex, but the 2NN FCC-HCP
72 motif is retained. At 1 ML the FCC-only configuration is lower in energy than HCP-only;
73 any mixed configuration would have high energy 1NN CO. As evident from Figure 3 D,
74 many other configurations are close in energy to the ground state hull. Figure 3 E plots
75 the differential binding energy $\bar{E}_{CO}^{F/H}(\theta)$ extracted from the ground state hull. Energies
76 increase in more gradual steps than in the FCC-only model up to 5/7 ML, where $\bar{E}_{CO}^{F/H}(\theta)$
77 jumps to a strongly positive value. Table 2 summarizes the structures for the ground states.
- 78 3. Figure 3 I shows a comparison of the DFT computed formation energies with the cluster
79 expansion predicted formation energies. Figure 3 G shows the DFT formation energies
80 with the formation energy hull, where there are “kinks” at 1/3, 1/2, 3/5, and 3/4 ML,
81 which correspond to the ground states. The ground states at 1/3, 1/2, 3/5 and 1 ML
82 are the same ground states determined in by the FCC, and HCP Hollow site cluster
83 expansion (Figure 2 C-F). A new ground state at 3/4 ML has CO adsorbed in a FCC
84 Hollow, HCP Hollow and Atop site. Figure 3 H shows the 0 K differential binding energy,
85 where there are steps at 0, 1/3, 1/2, 3/5, and 3/4 ML. At 3/4 ML, the 0 K differential
86 binding energy becomes positive, which is different from the previous models. Table 3
87 reports the geometric configurations for the ground states

88 GCMC Simulation Result

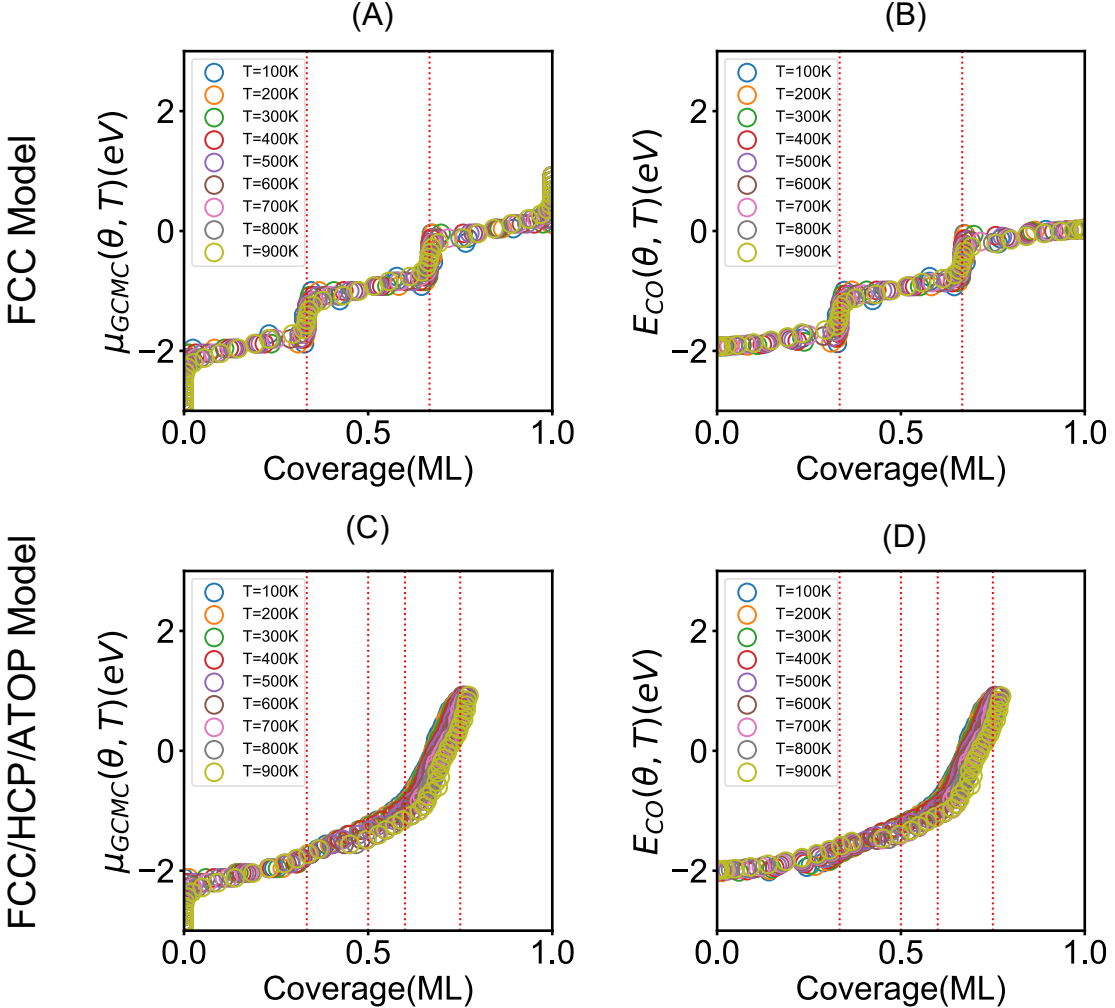


Figure 4: First column: $\mu_{CO}(\theta, T)$ vs. coverage for FCC model and FCC/HCP/ATOP models from top to bottom at temperature range from 100K to 900K. Last column: $E_{CO}(\theta, T)$ vs. coverage for the same models.

- 89 1. GCMC simulations were performed from 100K to 900K on the one-site and three-site CE
90 models. Results are shown in Figure 4 A and C, plotted as $\mu_{GCMC}(\theta, T)$ vs. θ_{CO} .
- 91 2. The chemical potential diverges in the limits of 0 and 1 ML, reflecting the divergence of
92 Eq. 2 in those limits. The one-site model (Figure 4 A) retains the 0 K stair-step pattern
93 smeared out at the boundaries of each ground states. The three site model (Figure 4 C)
94 shows a qualitatively different gradual rise in chemical potential to approximately 0.6 ML,
95 followed by a sharper rise from 0.6 to 0.75 ML.
- 96 3. Figure 4 B and D shows $\bar{E}_{CO}(\theta, T)$ vs. θ extracted using Eq. 1. Subtraction of the mean-
97 field configurational entropy eliminates the divergences at the extremes of coverage and

98 damps the rise in energy at intermediate coverage. Further, the sharp discontinuities
99 present in the 0 K differential binding energies are smeared out at finite temperature.
100 Figure 4 B and D show that the differential binding energies extracted this way are only
101 weakly temperature dependent.

102 Coverage-Dependent Binding Energy Models

103 FCC Model

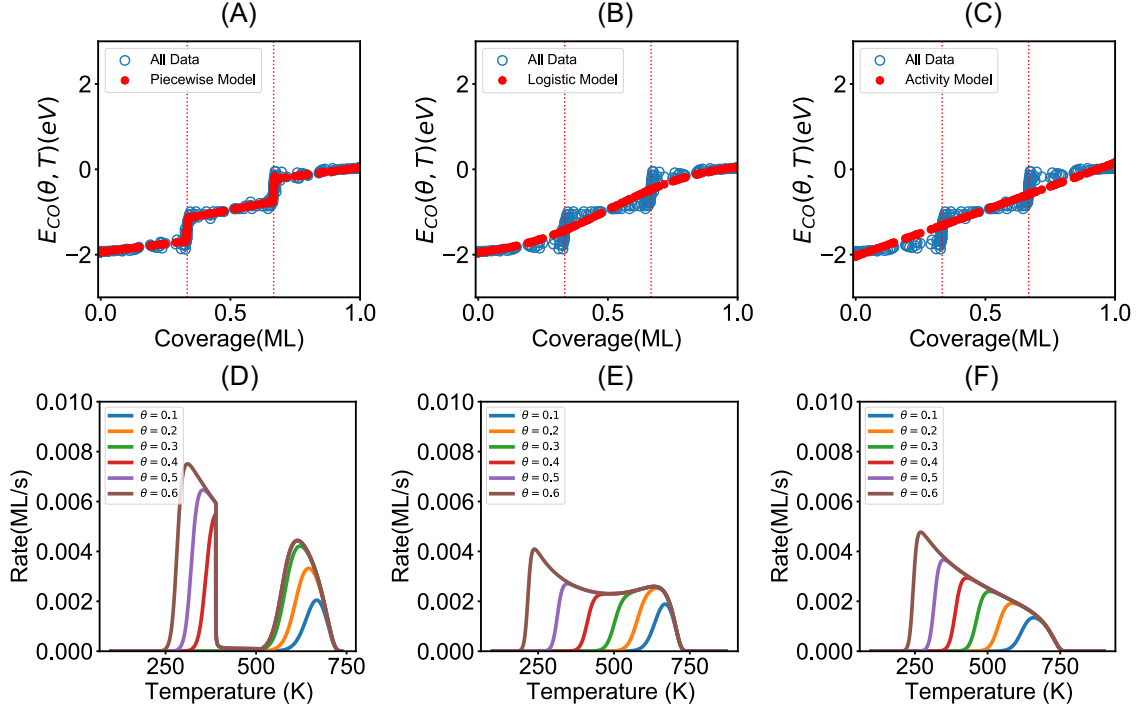


Figure 5: First column: piecewise model fit to all data point and correspond TPD plot. Second column: logistic model fit to all data point and correspond TPD plot. Third column: activity model fit to all data point and correspond TPD plot.

Table 4: Analytical Fitting Result for FCC Model

Model	R^2	MAE	MSE
Piecewise	0.977	0.0397	0.00391
Logistic	0.958	0.106	0.0218
Activity	0.938	0.145	0.0323

- 104 1. Figure 5 D has two different peak region below 400K and around 700K, which represent
 105 different binding energy when coverage above and below 0.3 ML. Figure 5 E has gradually
 106 changed shape that with initial θ increasing. Clear peak is about 700K at low coverage.
 107 Figure 5 F shows peak temperature shift lower when initial θ increase, indicate that
 108 binding energy keep decreasing. Although piecewise model has the highest R^2 value and
 109 lowest MAE and MSE, but TPD plot did not consistent with experimental TPD [4], it
 110 suggest that one site model is insufficient to simulate real TPD.

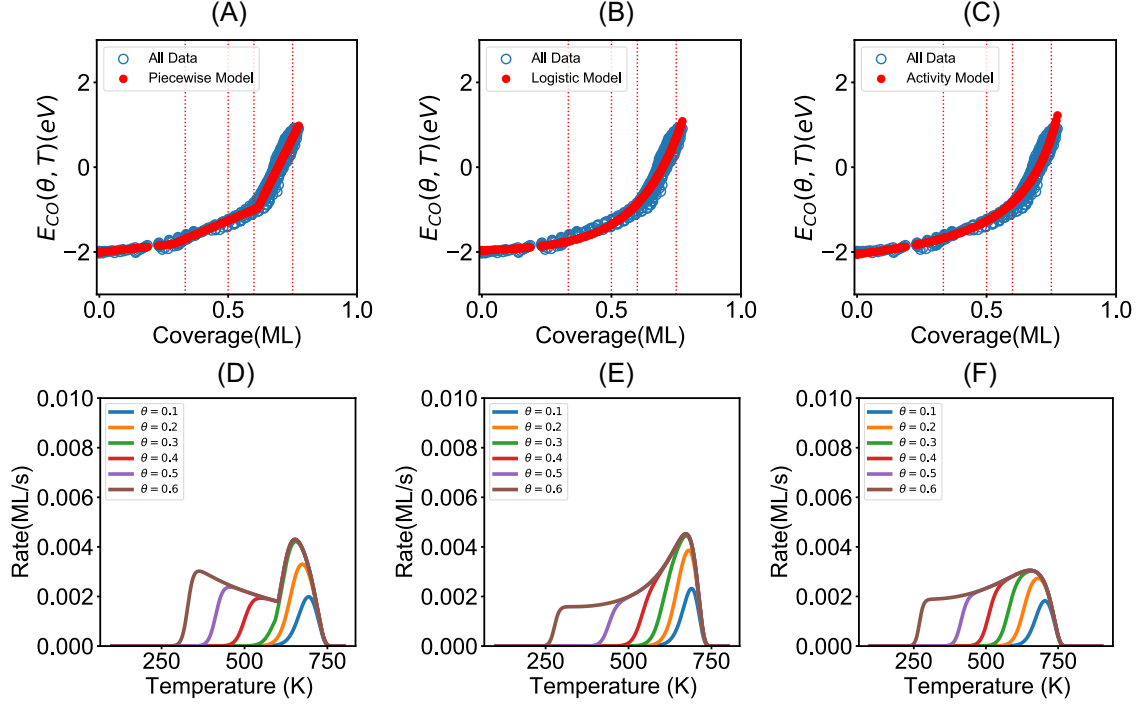


Figure 6: First column: linear model fit to all data point and correspond TPD plot. Second column: logistic model fit to all data point and correspond TPD plot. Third column: activity model fit to all data point and correspond TPD plot.

Table 5: Analytical Fitting Result for FCC/HCP/ATOP Model

Model	R ²	MAE	MSE
Piecewise	0.975	0.110	0.00224
Logistic	0.970	0.126	0.0265
Activity	0.968	0.126	0.0285

- 112 1. From Table 5, three model have similar R² value, but piecewise have lowest MAE and
113 MSE value. However, simulated TPD has irregular area when intial θ above 0.3 ML.
- 114 2. Logistic and activity model have similar fitting result and logistic model TPD figure has
115 general shape that consistent with experimental TPD. When initial θ below 0.3 ML,
116 desorption temperature peak is around 700K. When initial θ above 0.3 ML, it has long
117 leading edge represent gradually changed binding energy.
- 118 3. Compare Figure 6 E and F, TPD plot largely depend on fitting model.

₁₁₉ **Conclusion**

- ₁₂₀ 1. Simulation result of one site model can recover DFT-computed binding energy trend, but
₁₂₁ simulated TPD plot using three analytical model cannot recover features of experimental
₁₂₂ TPD.
- ₁₂₃ 2. Simulation result of two site and three site model cannot follows DFT-computed binding
₁₂₄ energy trend, but simulated TPD can recover general shape and high temperature peak
₁₂₅ using logistic model. Therefore, including multi-site is necessary to recover experimental
₁₂₆ TPD.
- ₁₂₇ 3. Three-site model can recover high temperature peak around 700K, which higher than
₁₂₈ 500K of experimental TPD, because DFT tend to over estimate binding energy on Pd
₁₂₉ surface. Further, accurate capture coverage-dependent binding energy can contribute to
₁₃₀ construct WGS microkinetic model.

¹³¹ **References**

- ¹³² (1) Grabow, L. C.; Hvolbæk, B.; Nørskov, J. K. Understanding Trends in Catalytic Activity:
¹³³ The Effect of Adsorbate-Adsorbate Interactions for CO Oxidation Over Transition Metals.
¹³⁴ *Topics in Catalysis* **2010**, *53*, 298–310.
- ¹³⁵ (2) Bajpai, A.; Frey, K.; Schneider, W. F. Comparison of Coverage-Dependent Binding Energy
¹³⁶ Models for Mean-Field Microkinetic Rate Predictions. *Langmuir* **2020**, *36*, 465–474.
- ¹³⁷ (3) Grabow, L. C.; Gokhale, A. A.; Evans, S. T.; Dumesic, J. A.; Mavrikakis, M. Mechanism
¹³⁸ of the Water Gas Shift Reaction on Pt: First Principles, Experiments, and Microkinetic
¹³⁹ Modeling. *The Journal of Physical Chemistry C* **2008**, *112*, 4608–4617.
- ¹⁴⁰ (4) Guo, X.; Yates, J. T. Dependence of Effective Desorption Kinetic Parameters on Surface
¹⁴¹ Coverage and Adsorption Temperature: CO on Pd(111). *The Journal of Chemical Physics*
¹⁴² **1989**, *90*, 6761.

¹⁴³ Supporting Information

¹⁴⁴ FCC Model

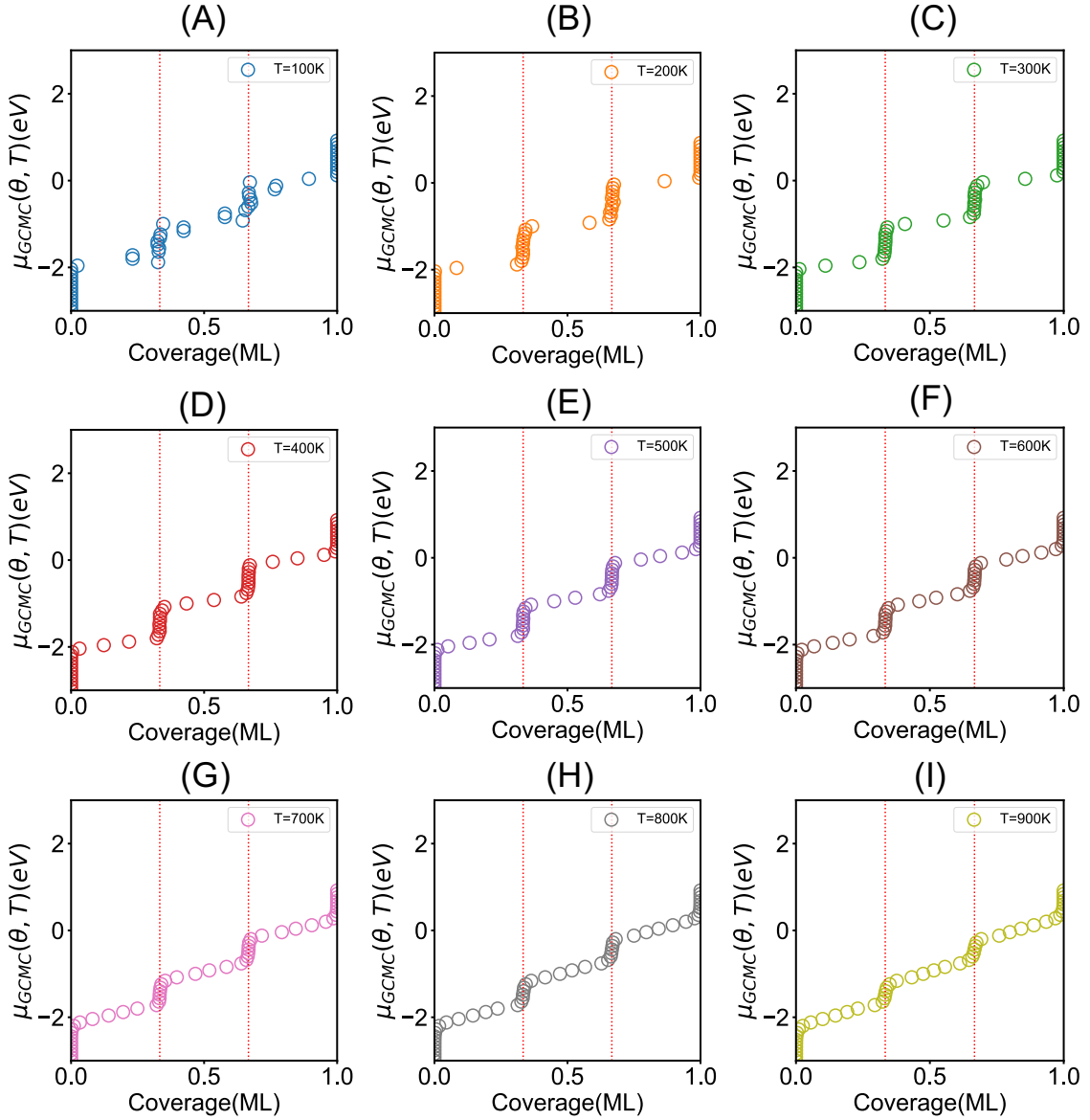


Figure 7: FCC Model simulation result of chemical potential μ vs. CO coverage from 100K to 900K. Red line represent ground state computed from DFT energy.

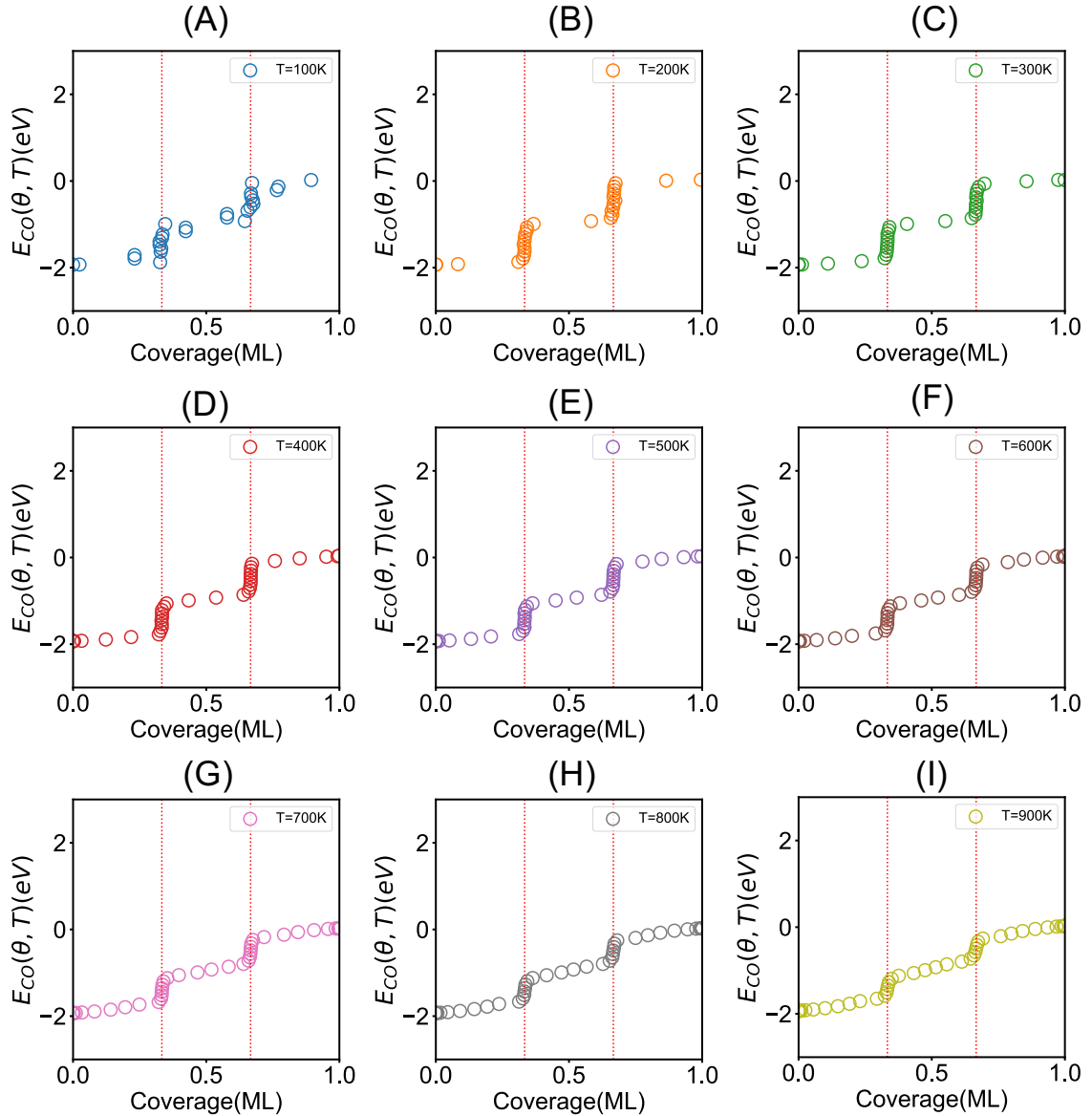


Figure 8: FCC Model binding energy vs. CO coverage from 100K to 900K after applying equation 1

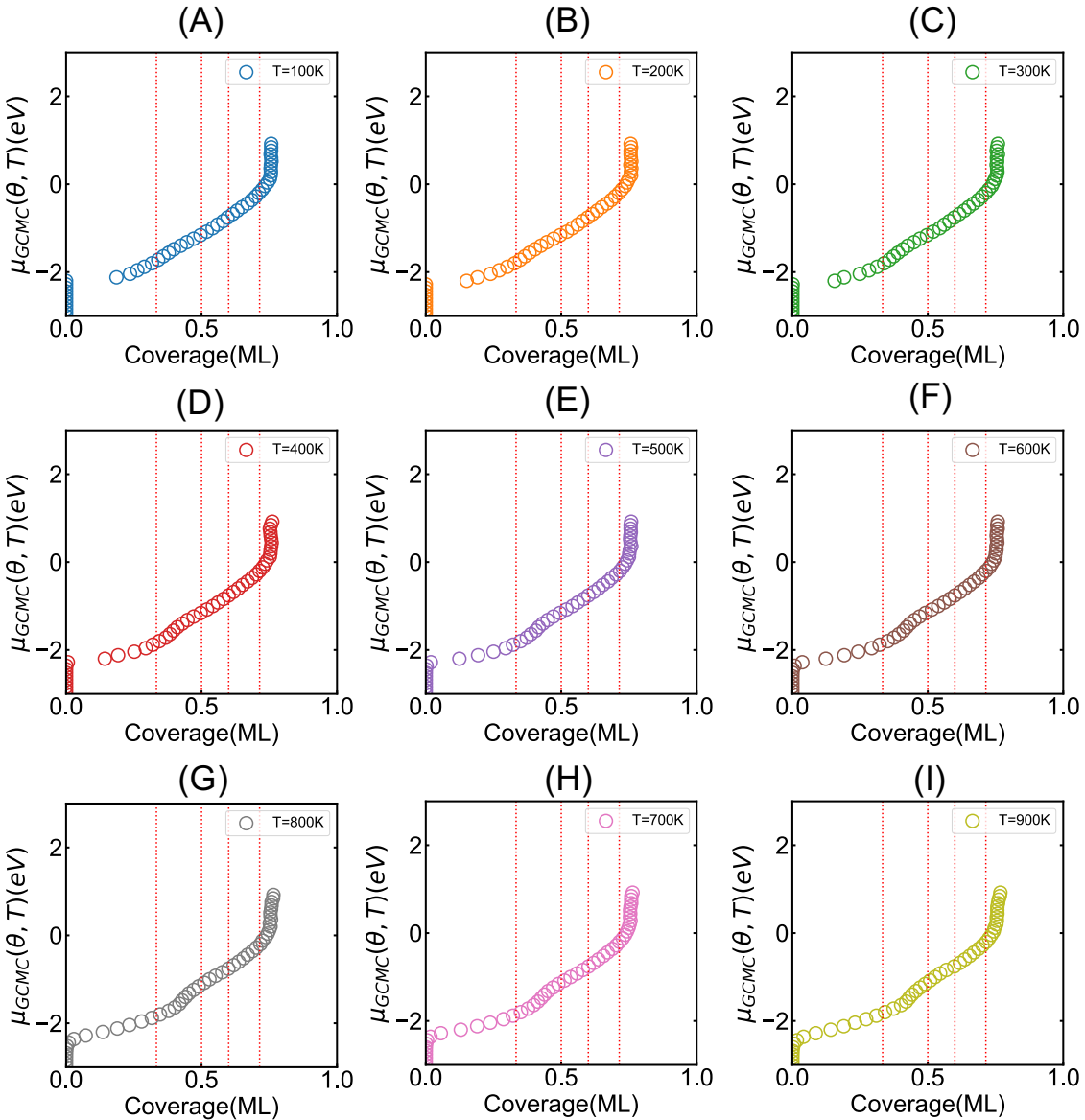


Figure 9: FCC/HCP Model simulation result of chemical potential μ vs. CO coverage from 100K to 900K. Red line represent ground state computed from DFT energy.

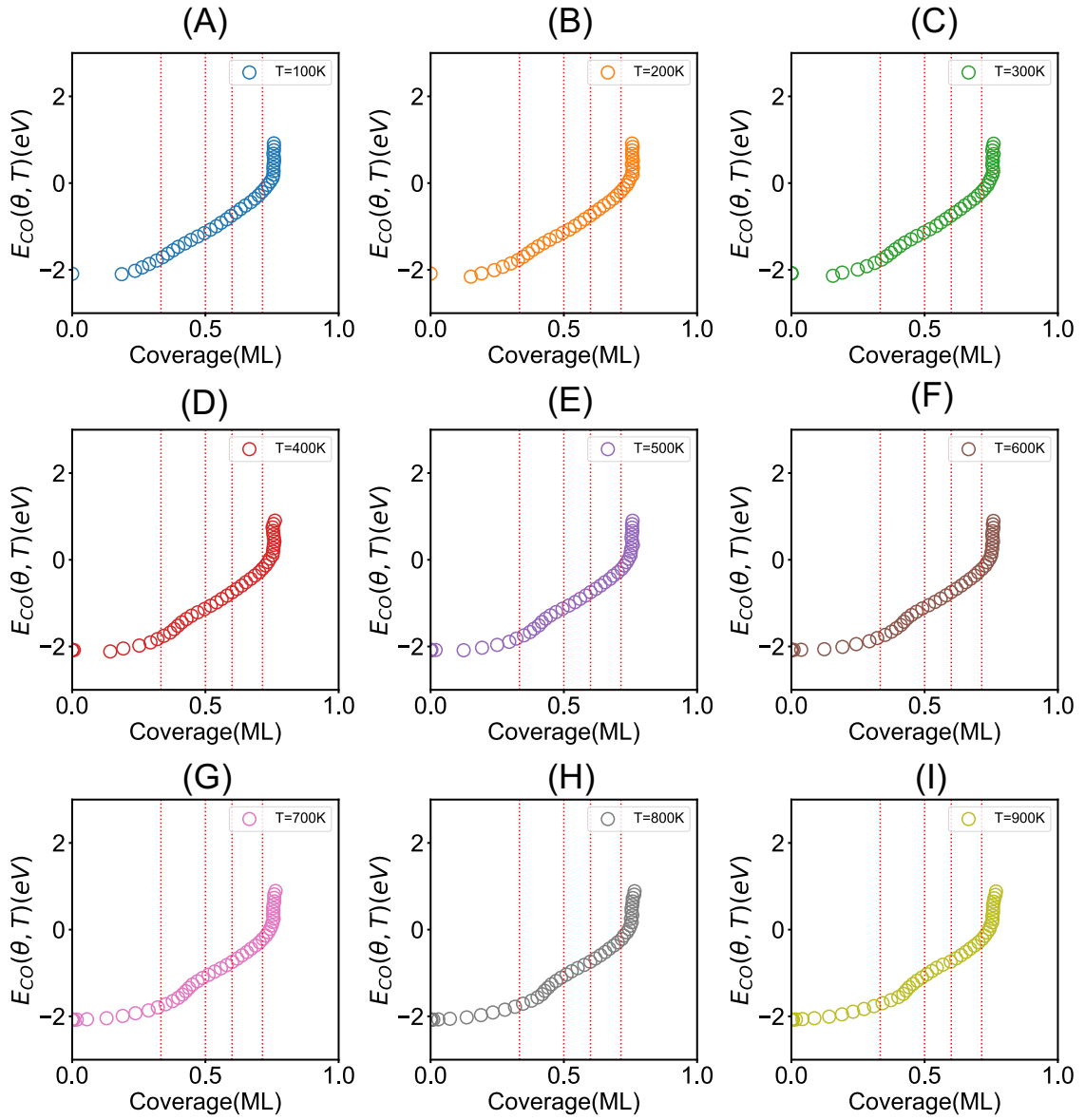


Figure 10: FCC/HCP Model binding energy vs. CO coverage from 100K to 900K after applying equation 1

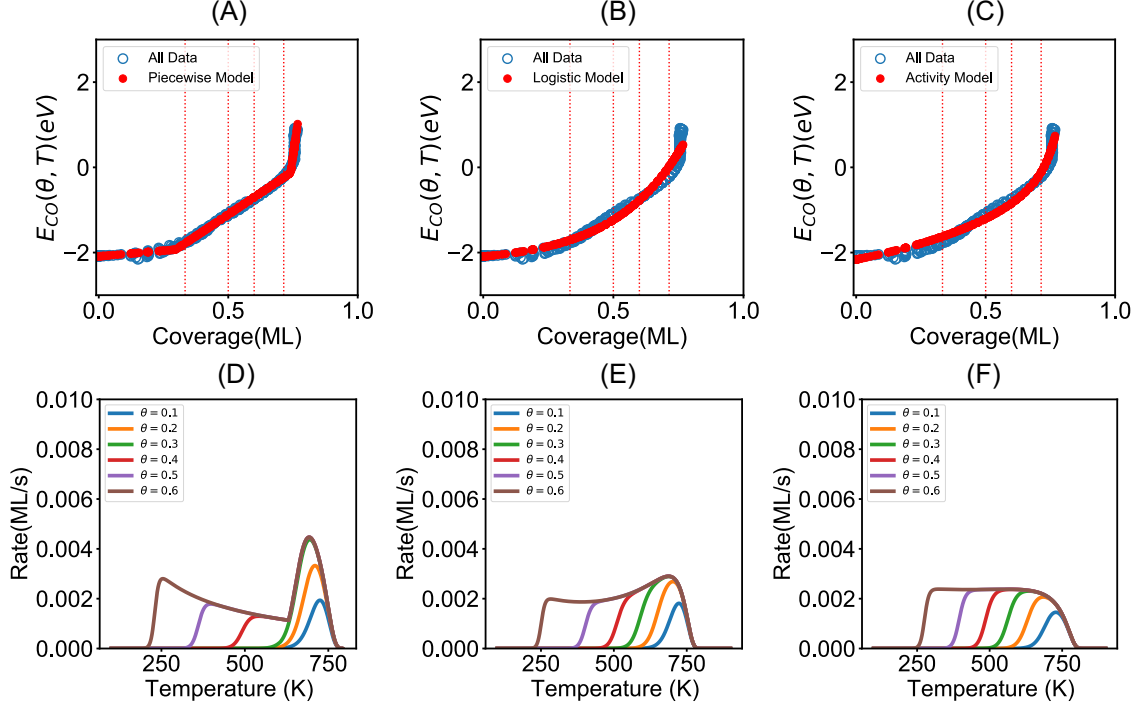


Figure 11: First column: linear model fit to all data point and correspond TPD plot. Second column: logistic model fit to all data point and correspond TPD plot. Third column: activity model fit to all data point and correspond TPD plot.

Table 6: Analytical Fitting Result for FCC/HCP Model

Model	R ²	MAE	MSE
Piecewise	0.989	0.0629	0.00987
Logistic	0.971	0.121	0.0261
Activity	0.978	0.118	0.0202

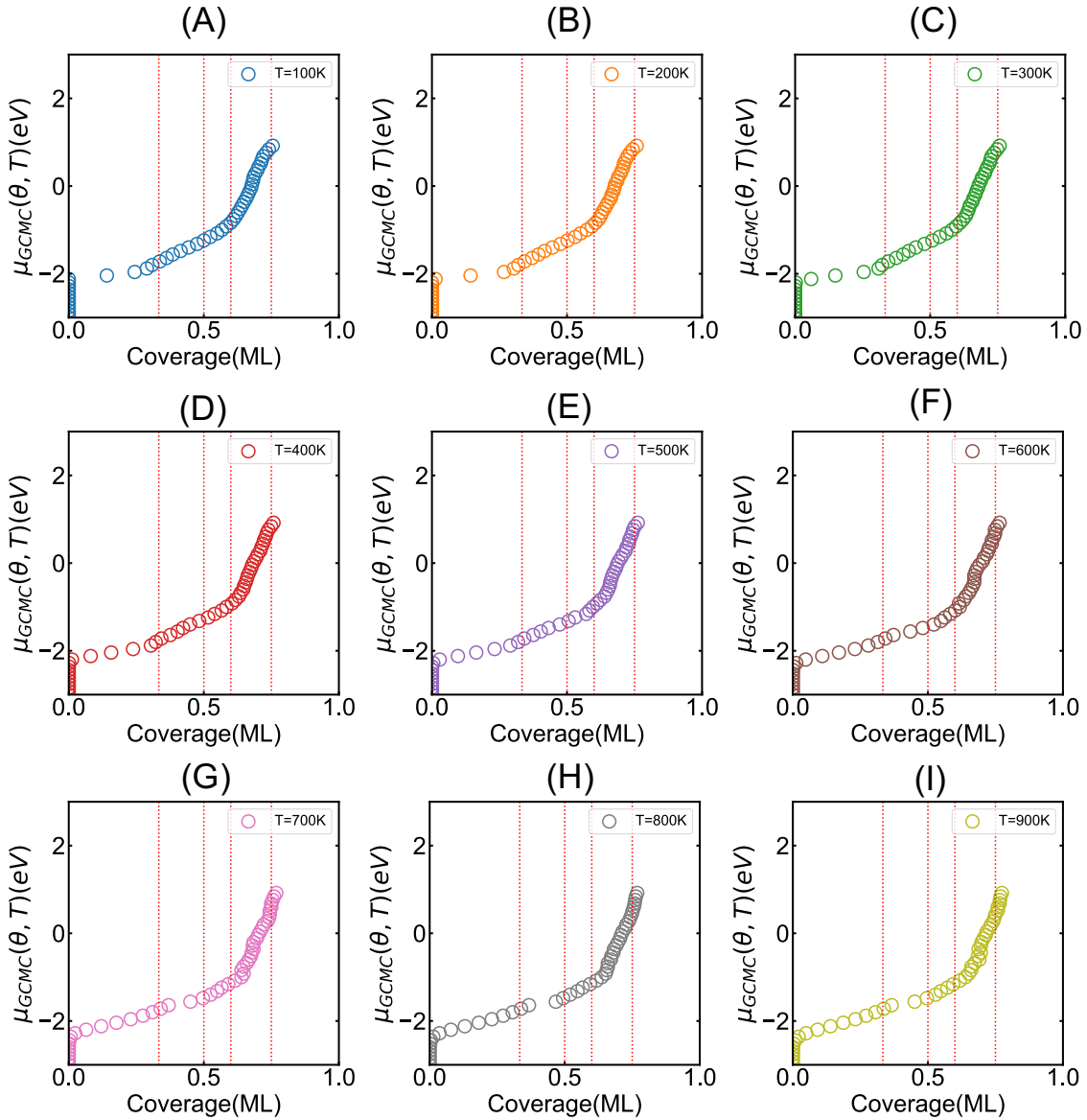


Figure 12: FCC/HCP/ATOP Model simulation result of chemical potential μ vs. CO coverage from 100K to 900K. Red line represent ground state computed from DFT energy.

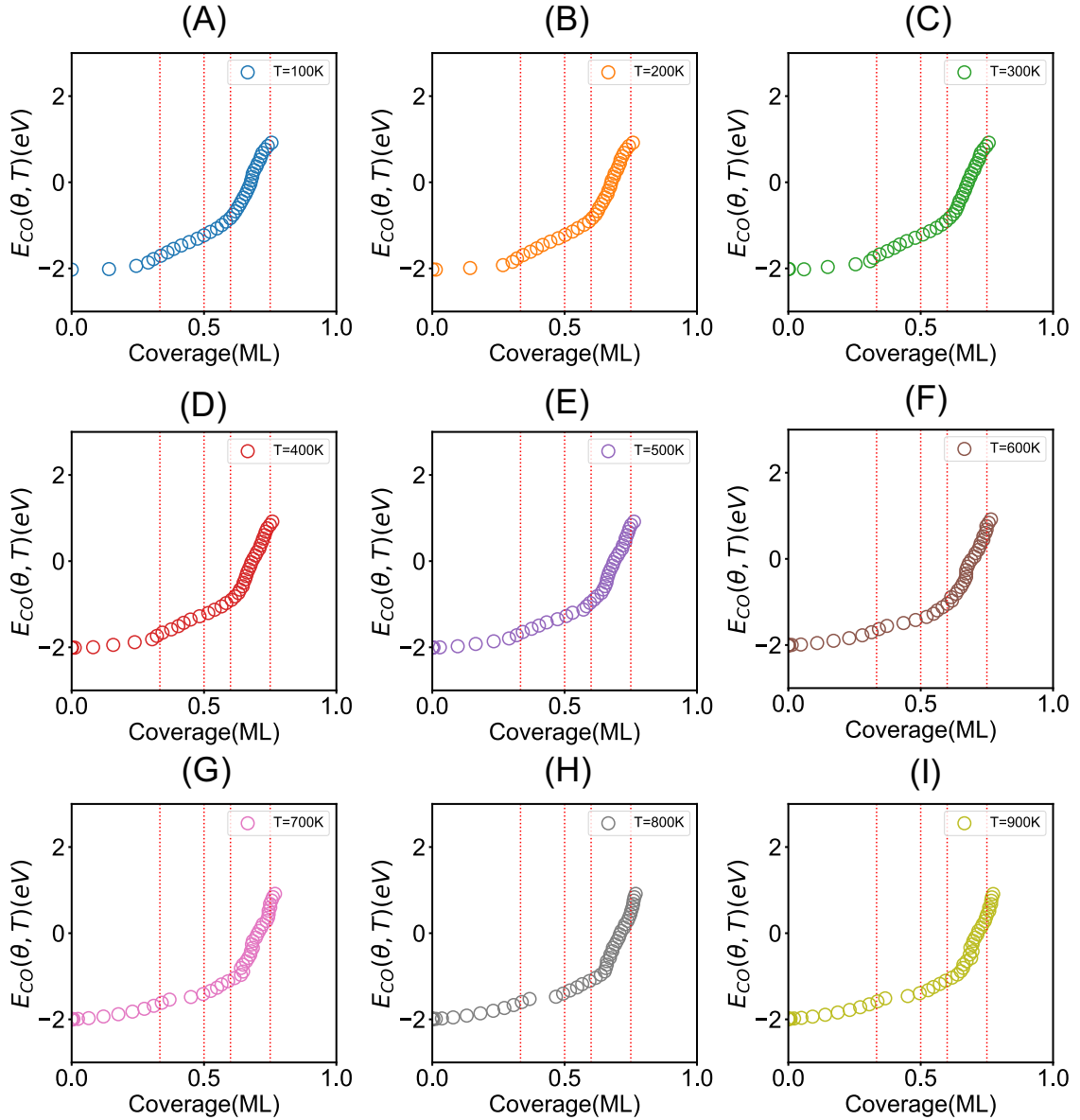


Figure 13: FCC/HCP/ATOP Model binding energy vs. CO coverage from 100K to 900K after applying equation 1